Exosomes mediate cell contact–independent ephrin-Eph signaling during axon guidance

Jingyi Gong,[1,3] Roman Körner,[2,3] Louise Gaitanos,[1] and Rüdiger Klein[1,3]

[1]Max Planck Institute of Neurobiology and [2]Max Planck Institute of Biochemistry, 82152 Martinsried, Germany
[3]Munich Cluster for Systems Neurology (SyNergy), 80336 Munich, Germany

The cellular release of membranous vesicles known as extracellular vesicles (EVs) or exosomes represents a novel mode of intercellular communication. Eph receptor tyrosine kinases and their membrane-tethered ephrin ligands have very important roles in such biologically diverse processes as neuronal development, plasticity, and pathological diseases. Until now, it was thought that ephrin-Eph signaling requires direct cell contact. Although the biological functions of ephrin-Eph signaling are well understood, our mechanistic understanding remains modest. Here we report the release of EVs containing Ephs and ephrins by different cell types, a process requiring endosomal sorting complex required for transport (ESCRT) activity and regulated by neuronal activity. Treatment of cells with purified EphB2$^+$ EVs induces ephrinB1 reverse signaling and causes neuronal axon repulsion. These results indicate a novel mechanism of ephrin-Eph signaling independent of direct cell contact and proteolytic cleavage and suggest the participation of EphB2$^+$ EVs in neural development and synapse physiology.

Introduction

The ephrin-Eph signaling system is a bidirectional cell–cell communication device mediated by membrane-tethered ligand–receptor interactions. Ephs and ephrins function in many different physiological processes, including boundary formation and axon guidance, as well as pathological processes such as cancer (Klein and Kania, 2014).

Ephs and ephrins fall into two subclasses, with EphAs mostly interacting with glycosylphosphatidylinositol-linked ephrinAs and EphBs mostly interacting with transmembrane ephrinBs. The classic mode of signaling, from ephrins to Ephs (ephrin:Eph), is referred to as forward signaling. Ephs can also act as ligands for ephrins (Eph:ephrin), which is known as reverse signaling (Klein and Kania, 2014). Ephrin-Eph signaling at the interface between two opposing cells involves the formation of higher-order clusters, and the degree of Eph clustering may determine whether cells are repelled from or adhere to each other (Seiradake et al., 2013; Schaupp et al., 2014). Two mechanisms have been described for ephrin-Eph–mediated separation during cell–cell repulsion: (1) transendocytosis of the ligand–receptor complex, often by both opposing cells (Marston et al., 2003; Zimmer et al., 2003), and (2) proteolytic cleavage and ectodomain shedding, which breaks the molecular tether between two opposing cells (Hattori et al., 2000; Janes et al., 2005, 2009; Georgakopoulos et al., 2006; Gatto et al., 2014). Because unclustered Ephs and ephrins

are weak agonists of their respective binding partners (Davis et al., 1994), the soluble and unclustered shed products are likely unable to activate ephrin-Eph signaling from afar.
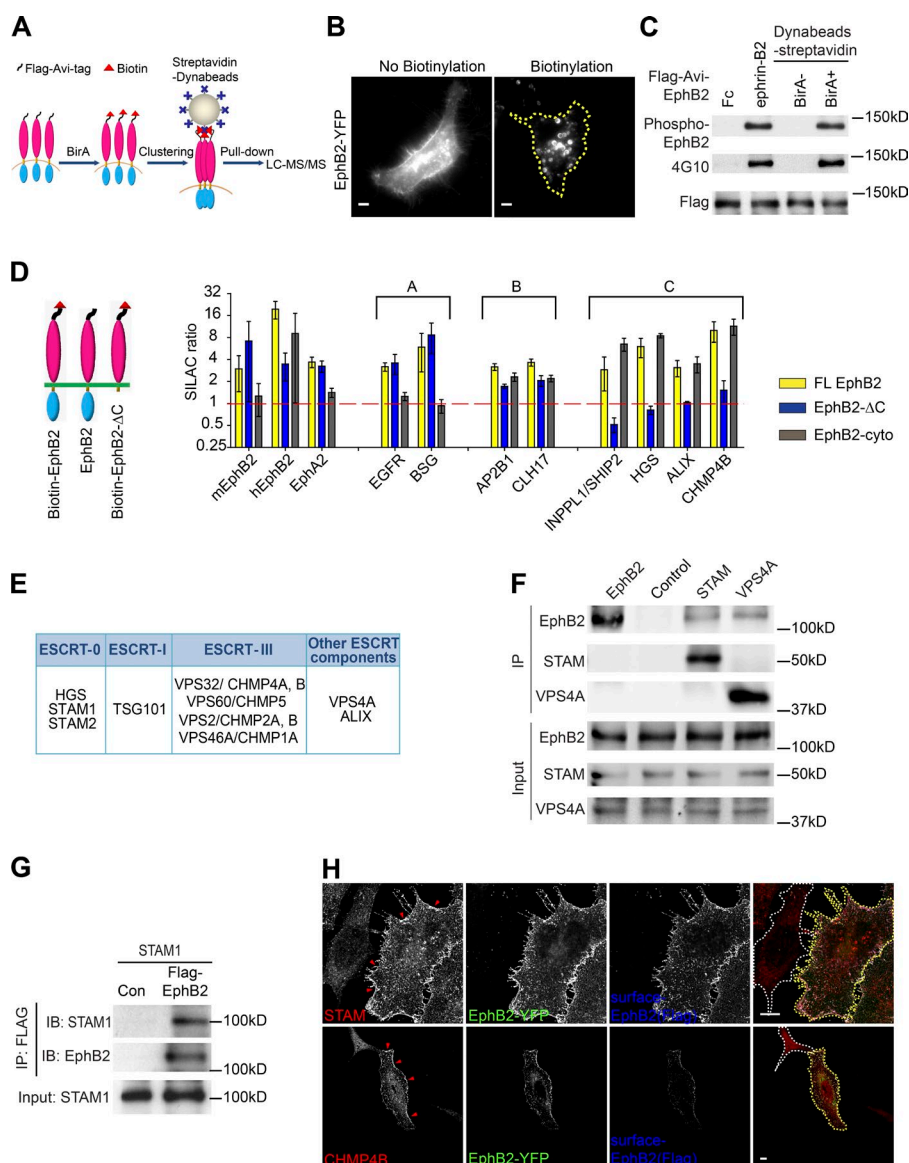
Extracellular vesicles (EVs) have emerged as vectors of genetic information and can induce changes in the physiologic state of cells (Tkach and Théry, 2016). They are released by essentially all cells of the nervous system (Rajendran et al., 2014) and have been implicated in synaptic growth (Korkut et al., 2013) and pruning (Bahrini et al., 2015). Exosomes are small EVs distinguished from other vesicles by size (40–200 nm in diameter), endosomal origin, and composition (Colombo et al., 2014). They are formed by budding into multivesicular bodies (MVBs) and fusion to the plasma membrane, a process requiring the endosomal sorting complex required for transport (ESCRT), a conserved machinery consisting of four subcomplexes (ESCRT-0, -I, -II, and -III) with associated proteins such as ALIX (Colombo et al., 2013). Proteome profiling of exosomes has indicated the presence of Eph and ephrin family members (Li et al., 2013; Tauro et al., 2013; Barile et al., 2014), but the functional relevance of these observations has been unclear.

Here, we analyzed the interactome of clustered EphB2 and identified members of the ESCRT complex as EphB2 interactors. Interestingly, we found that endogenous Ephs and ephrins are released to EVs from glioblastoma U-251MG cells and primary neurons. Moreover, EphB2-containing EVs are taken up by ephrinB1$^+$ cells, inducing ephrinB1 tyrosine phosphorylation

---

The Rockefeller University Press $30.00
J. Cell Biol. Vol. 214 No. 1   35–44
www.jcb.org/cgi/doi/10.1083/jcb.201601085

JCB   35

Figure 1. **Proteomic screen identifies ESCRT components as EphB2 interactors.** (A) Strategy of purification and identification of the interactome of biotinylated EphB2 by mass spectrometry. (B) Representative images showing clustering of biotinylated FLAG-Avi-EphB2-YFP fusion protein around streptavidin-conjugated Dynabeads (within 5 min, right, stippled line). This effect required EphB2 biotinylation (left). (C) Western blot analysis showing tyrosine autophosphorylation (detected by anti-phospho EphB2 [Y594] or 4G10 antibodies) of biotinylated (BirA+) but not unbiotinylated (BirA−) FLAG-Avi-EphB2 in response to incubation with streptavidin-conjugated Dynabeads. Unfused Fc protein was used as negative control. Similar results were observed in three independent replicates. (D) Bar graph showing the SILAC ratios of representative members of different groups of the top 30 enriched full-length EphB2 interactors ($n = 3$, mean ± SEM). Yellow, biotinylated versus unbiotinylated full-length EphB2 (FL EphB2); blue, biotinylated EphB2-ΔC versus unbiotinylated full-length EphB2 (EphB2-ΔC); gray, biotinylated full-length EphB2 versus biotinylated EphB2-ΔC (EphB2-cyto). (E) Full list of ESCRT complex components identified in the proteomic screen as interactors of full-length EphB2 in at least one of the three replicates. (F) Validation of the interaction between EphB2 and endogenous STAM1 or VPS4A by co-IP/Western blot (WB) analysis in HEK293 cells stably expressing EphB2. (G) Validation of the interaction between overexpressed EphB2 and STAM1 in HeLa cells. (H) Representative images showing that endogenous STAM and CHMP4B colocalize with surface EphB2 in HeLa cells. STAM and CHMP4B levels at the plasma membrane were increased 3.5- and 2-fold, respectively (highlighted by red triangles), in EphB2+ cells (indicated by yellow stippled line in the merge) compared with untransfected cells (white stippled line). Bars, 10 μm.
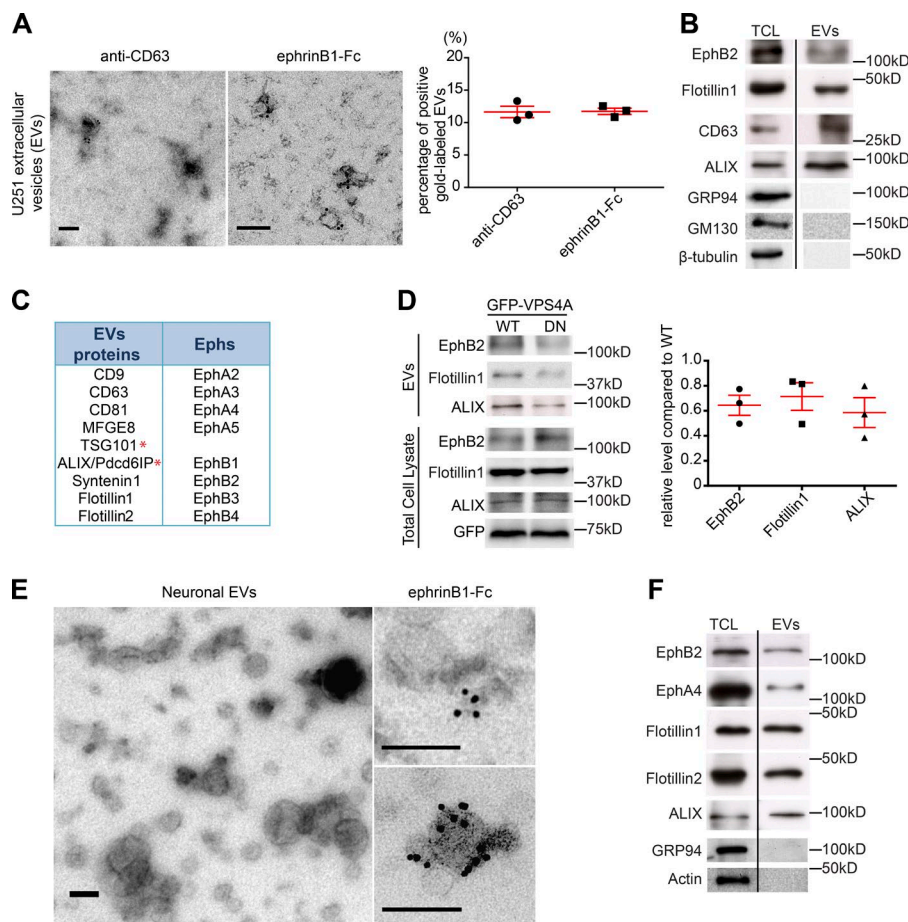
and triggering neuronal growth cone collapse. These findings uncover a novel theory that Ephs and ephrins can signal at a distance via EVs, in addition to the canonical bidirectional signaling that depends on cell–cell contact.

Results and discussion

To characterize the initial events leading to EphB2 endocytosis, we identified the interactome of clustered EphB2 in the plasma membrane by inducing EphB2 clustering on the cell surface with beads too large to be internalized (Fig. 1, A and B; and not depicted). This excluded enrichment of proteins that preferentially interacted with EphB2 in intracellular vesicles. Surface EphB2 clustering with beads induced EphB2 autophosphorylation in a fashion similar to that of soluble preclustered ephrinB2-Fc fusion protein, confirming functional signaling (Fig. 1 C). For proteome profiling of EphB2 interactors, we first compared HeLa cells expressing biotinylated versus unbiotinylated EphB2. To distinguish interactors of EphB2 ecto- and cytoplasmic domains, we compared cells expressing full-length EphB2

versus EphB2 lacking its entire intracellular part (EphB2-ΔC). Stable isotope labeling by amino acids in cell culture (SILAC; Ong et al., 2002) with light, medium, and heavy forms of arginine and lysine allowed accurate quantitation of protein ratios in these three samples. As confirmation, endogenous (human) EphB2 and EphA2 were found among the top 30 interactors of full-length (mouse) EphB2 (Fig. 1 D).

Interactors were classified into different groups according to their preference for full-length EphB2, EphB2-ΔC, or both. Group A interacted equally well with full-length EphB2 and EphB2-ΔC and contained exclusively cell surface, transmembrane proteins. Group B interacted better with full-length EphB2 than EphB2-ΔC, but was also enriched after pull-down with biotinylated EphB2-ΔC versus unbiotinylated control. This group contained mediators of endocytosis including clathrin (CLH17) and AP2 complex proteins (AP2B1). Group C showed a clear preference for the EphB2 cytoplasmic domain and was not enriched in biotinylated EphB2-ΔC versus control. Notably, this group contained SHIP2, a previously described mediator of Eph signaling (Zhuang et al., 2007), as well as components of the ESCRT complex, including HGS, ALIX, and

A

U251 extracellular vesicles (EVs)

anti-CD63 | ephrinB1-Fc

(%)

percentage of positive gold-labeled EVs

anti-CD63 | ephrinB1-Fc

B

	TCL	EVs	
EphB2			—100kD
			—50kD
Flotillin1			—50kD
CD63			—25kD
ALIX			—100kD
GRP94			—100kD
GM130			—150kD
β-tubulin			—50kD

Figure 2. **Ephs and ephrins released via EVs.** (A) Representative IEM images and quantification of purified EVs from U251 cells with anti-CD63 antibody or ephrinB1-Fc protein labeling. Control Fc protein gave no specific signal (data not shown; data from three separate EV preparations and IEM experiments). (B) Western blot (WB) analysis of U251 total cell lysate (TCL) and EV fraction with the indicated antibodies. GRP94, GM130, and β-tubulin are absent in purified EVs and are used as quality control. Similar results were observed in three independent replicates. (C) List of EV and ESCRT proteins (with asterisk) and Ephs in U251 EVs by proteomic analysis. (D) WB analysis of TCL and EV fractions derived from U251 cells expressing either wild-type GFP-VPS4A (WT) or dominant-negative GFP-VPS4A^{E228Q} (DN) with the indicated antibodies (left). Quantification of the levels of EphB2, Flotillin1, and ALIX in EVs from cells expressing DN-VPS4A normalized to EVs from WT-VPS4A expressing cells (right). (E) Representative EM image of purified EVs from E15.5 dissociated motor cortex neurons kept (14 DIV; left). IEM pictures using ephrinB1-Fc under nonpermeabilizing conditions (right). (F) WB analysis of cultured neuron TCL and EV fraction with indicated antibodies. Similar results were observed in three independent replicates. Bars, 100 nm.

C

EVs proteins	Ephs
CD9	EphA2
CD63	EphA3
CD81	EphA4
MFGE8	EphA5
TSG101 *	
ALIX/Pdcd6IP *	EphB1
Syntenin1	EphB2
Flotillin1	EphB3
Flotillin2	EphB4

D

GFP-VPS4A
WT | DN

EVs
EphB2	—100kD
Flotillin1	—37kD
ALIX	—100kD

Total Cell Lysate
EphB2	—100kD
Flotillin1	—37kD
ALIX	—100kD
GFP	—75kD

relative level compared to WT

EphB2 | Flotillin1 | ALIX

E

Neuronal EVs | ephrinB1-Fc

F

	TCL	EVs	
EphB2			—100kD
EphA4			—100kD
			—50kD
Flotillin1			—50kD
Flotillin2			—50kD
ALIX			—100kD
GRP94			—100kD
Actin			—50kD

CHMP4B (Fig. 1 D and Fig. S1 A; Rusten et al., 2011). In total, at least 200 proteins were identified in all three SILAC replicates (Table S1). Individual log$_2$ values of the SILAC ratios for all identified proteins in each replicate showed high consistency among the three SILAC proteomic replicates (Fig. S1 B). In summary, our proteomic analysis identified several members of the ESCRT complex, and they all belong to Group C (Fig. 1 E).

To validate the interaction between EphB2 and ESCRT proteins, we coimmunoprecipitated EphB2 with endogenous signal-transducing adaptor molecule (STAM) or VPS4A from HEK293 cells stably expressing EphB2 (Fig. 1 F). Similarly, STAM, CHMP4B, and VPS4A were coimmunoprecipitated using FLAG-tagged EphB2 from transfected HeLa cells (Fig. 1 G and Fig. S1, C and D). Further, we demonstrated the interaction of endogenous STAM and CHMP4B with overexpressed EphB2 by immunofluorescence analysis. Endogenous STAM and CHMP4B were mostly located throughout the cytoplasm in naive HeLa cells. Upon overexpression of EphB2, endogenous STAM and CHMP4B were enriched in the plasma membrane, where they colocalized with surface EphB2 (Fig. 1 H). When EphB2 was clustered and trans-endocytosed upon contact with an opposing ephrinB1-expressing cell (Zimmer et al., 2003), STAM and CHMP4B partially colocalized with EphB2/ephrinB1 clusters and internalized vesicles (Fig. S1, E–H). These results indicate that components of the ESCRT complex interact with clustered EphB2.

These results raised the possibility that EphB2 was sorted into MVBs and packaged into EVs. To test this, we purified EVs from conditioned culture medium of human glioblastoma U-251MG cells endogenously expressing various Ephs (Nievergall et al., 2010). Immunoelectron microscopy (IEM) analysis of the P100 fraction (see Materials and methods) showed enrichment of cup-shaped vesicles of typical exosome sizes (40–200 nm in diameter) that stained positive (12%) for the exosome marker CD63. The labeling efficiency was relatively low, possibly because of the heterogeneity of the purified EV fraction and the technical limitation of IEM analysis in EVs (Tkach and Théry, 2016). IEM analysis of EVs under nonpermeabilizing conditions with ephrinB1-Fc, but not control Fc, revealed the presence of EphBs in the correct topology for ligand binding (Fig. 2 A, 12%). Western blot analysis using exosome markers confirmed the presence of EphB2 in the P100 fraction. The purity of the P100 fraction was confirmed by the absence of non–exosome-associated proteins such as ER protein GRP94, Golgi protein GM130, and β-actin (Fig. 2 B). Mass spectrometry of purified U-251MG EVs identified ~800 proteins (with two or more peptides identified), including exosome and ESCRT proteins (Simpson et al., 2012), as well as most Eph receptors (Fig. 2 C and Table S2).

To investigate whether the ESCRT machinery was necessary for EV release of EphB2, we purified EVs from conditioned medium of U251MG cells transiently overexpressing either wild-type GFP-VPS4A or dominant-negative GFP-VPS4A^{E228Q} (dnVPS4A; Kunadt et al., 2015). EV release into the culture supernatant, as judged by anti–Flotillin-1 and anti-ALIX immunoblotting, was significantly reduced by the expression of dnVPS4A. Endogenous EphB2 levels in EVs were also reduced, indicating that EV release of EphB2 requires the ESCRT

component VPS4 (Fig. 2 D). Similar results were obtained from HEK293 cells stably expressing EphB2 (Fig. S2 A). These results demonstrate release of EVs containing endogenous Ephs from glioblastoma cells and suggest that the interaction between EphB2 and ESCRT components contributes to this process.

Next we attempted to identify Ephs and ephrins in EVs released by cultured cortical neurons. IEM analysis revealed EVs containing EphB receptors based on ephrinB1-Fc versus control Fc staining (Fig. 2 E and not depicted). Western blot analysis showed the presence of EphB2 and EphA4 along with several exosome markers (Fig. 2 F). Mass spectrometry analysis identified ~3,300 proteins (with two or more peptides identified; Table S3), including exosome and ESCRT proteins, as well as most EphAs, EphBs, and ephrinBs. The presence of peptides derived from their ecto- and cytoplasmic domains demonstrated that full-length Ephs and ephrins were released via EVs rather than merely their shed ectodomains (Table S4). These results confirm the presence of Ephs and ephrins in purified EVs derived from cultured neurons.

To begin testing the function of EVs containing Ephs or ephrins, we purified large quantities of EVs from the conditioned media of HEK293 cells stably expressing EphB2 or HA-tagged ephrinB1. IEM and Western blot analysis against the exosome marker ALIX confirmed exosome/EV identity (Fig. 3, A and B; and Fig. S2, B and C). Quantification of the fraction of gold-labeled EVs revealed that 12% of EVs were positively labeled with anti-ALIX antibodies. IEM of purified EVs using specific anti-EphB2 and anti-HA antibodies indicated that 27% and 10% of EVs were positive for EphB2 and ephrinB1, respectively (Fig. 3, A and B; and Fig. S2 C), in contrast to purified EVs from naive HEK293 cells (<0.1% stained positive for EphB2 or HA; not depicted). Similar results were obtained for EphB2 and ephrinB1 EVs by Western blot analysis (Fig. S2 B). IEM of EphB2 and ephrinB1 EVs before permeabilization revealed specific binding of ephrinB1-Fc and EphB2-Fc, respectively, compared with Fc control protein (Figs. 3 A and S2 C and not depicted). Next, we asked whether EphB2+ EVs colocalize with membrane-bound ephrinB1 when applied to ephrinB1-expressing HeLa cells. Immunohistochemistry revealed that EphB2+ EVs bound more readily to cells expressing ephrinB1 (Fig. 3 C1) than to ephrinB1-negative cells (Fig. 3 C2) and that EphB2-labeled puncta colocalized with ephrinB1 clusters. To investigate whether, upon binding to ephrinB1, EphB2+ EVs would be taken up by the cells, we purified EphB2-containing EVs from HEK293 cells coexpressing membrane-targeted GFP. Most GFP-positive puncta were positive for EphB2, colocalized with internalized ephrinB1, and were largely excluded from ephrinB1 puncta on the cell surface (Fig. S2 D), suggesting that they were internalized by the cells.

Next we investigated whether EphB2+ EVs were able to initiate ephrinB reverse signaling. Incubation of SKN neuroblastoma cells endogenously expressing ephrinBs (unpublished data) with EphB2+ EVs induced tyrosine phosphorylation of ephrinBs. When the expression of ephrinB1 and ephrinB2 was knocked down in the cells by RNAi (~60% knockdown efficiency), tyrosine phosphorylation of ephrinBs was abolished (Fig. 3 D). These results suggest that EphB2+ EVs activate ephrinB reverse signaling when interacting with ephrinB-expressing cells.

Release of EphB2+ EVs by embryonic neurons raised the possibility that these EVs contribute to ephrin-Eph–mediated repulsive axon guidance. We therefore tested whether EphB2+ EVs could trigger the collapse of growth cones. Incubation of embryonic day 15.5 (E15.5) dissociated mouse forebrain neurons (3 days in vitro [DIV]) with EphB2+ EVs or soluble preclustered EphB2-Fc (as a positive control) induced significant growth cone collapse compared with control conditions (Fig. 4, A and B). Quantification of the mean growth cone area also revealed significant reductions in the presence of EphB2+ EVs (Fig. 4 C). We next tested the activity of EphB2+ EVs on the growth cones of neuronal tissue explants (Seiradake et al., 2014). We found that the growth cones of E15.5 mouse motor cortex explants (3 DIV) collapsed upon incubation with EphB2+ EVs compared with control EVs (Fig. 4, D and E). Because EphB2+ EVs were marked with GFP, we could quantify the ratio of collapsed growth cones in contact with GFP+/EphB2+ EVs compared with that of EV-free growth cones. We found that more than 80% of the growth cones in contact with EphB2+ EVs collapsed, in comparison to just over 40% of the growth cones without EV contact (Fig. 4, F and G). Collectively, these results indicate that EphB2+ EVs induce growth cone collapse and elicit physiological responses in neurons.

Exosome/EV release from cortical neurons has previously been shown to be enhanced by depolarization (Fauré et al., 2006), and it has been suggested that exosomes/EVs regulate intercellular communication in neural systems (Rajendran et al., 2014). To investigate whether the release of EphB2+ EVs is enhanced by membrane depolarization, we exposed mature cultures of cortical neurons to high KCl, depolarizing the plasma membrane and resulting in cascades of intracellular signaling. Dense cultures prepared from E15.5 mouse cortex (14 DIV) were incubated in basal medium with or without addition of 25 mM KCl for 1 h. Media were collected, replaced with fresh basal media, collected again after 6 and 30 h, and subjected to EV purification. According to the exosome marker flotillin1, EV release was enhanced by high KCl (Fig. 5, A and C). Likewise, the abundance of EphB2 protein in the exosome/EV preparations increased significantly (Fig. 5, A and B), suggesting that membrane depolarization enhances EV release, including EphB2+ EVs.

We show here that full-length Ephs and ephrins are present in EVs derived from different cell types, in the same topology as a cell that allows interaction with their cognate binding partners. Purified EphB2+ EVs are functional such that they preferentially bind to cells expressing ephrinB1, inducing ephrinB1 reverse signaling and neuronal growth cone collapse ex vivo. These results raise the interesting possibility that ephrin-Eph signaling may not be limited to cell–cell contact sites but also may occur at a distance. EVs are able to travel distances to participate in intercellular communication processes and have previously been suggested to regulate morphogen signaling and gradient formation (Sheldon et al., 2010; Gross et al., 2012; Gradilla et al., 2014). Further work is necessary to establish whether Eph/ephrin+ EVs participate in the formation of gradients and in repulsive axon guidance at intermediate targets (Klein and Kania, 2014).

With respect to cellular mechanisms, we demonstrate that endogenous ESCRT proteins bind to EphB2 and that EphB2 release via EVs requires at least one of the ESCRT components, namely VPS4A. Similarly, active Wnt is secreted through exosomes/Evs, depending on the ESCRT-mediated MVB sorting pathway (Gross et al., 2012). We also provide the first evidence that EV release of EphB2 is enhanced by membrane depolarization of mature neurons, raising the possibility that EphB2+ EVs
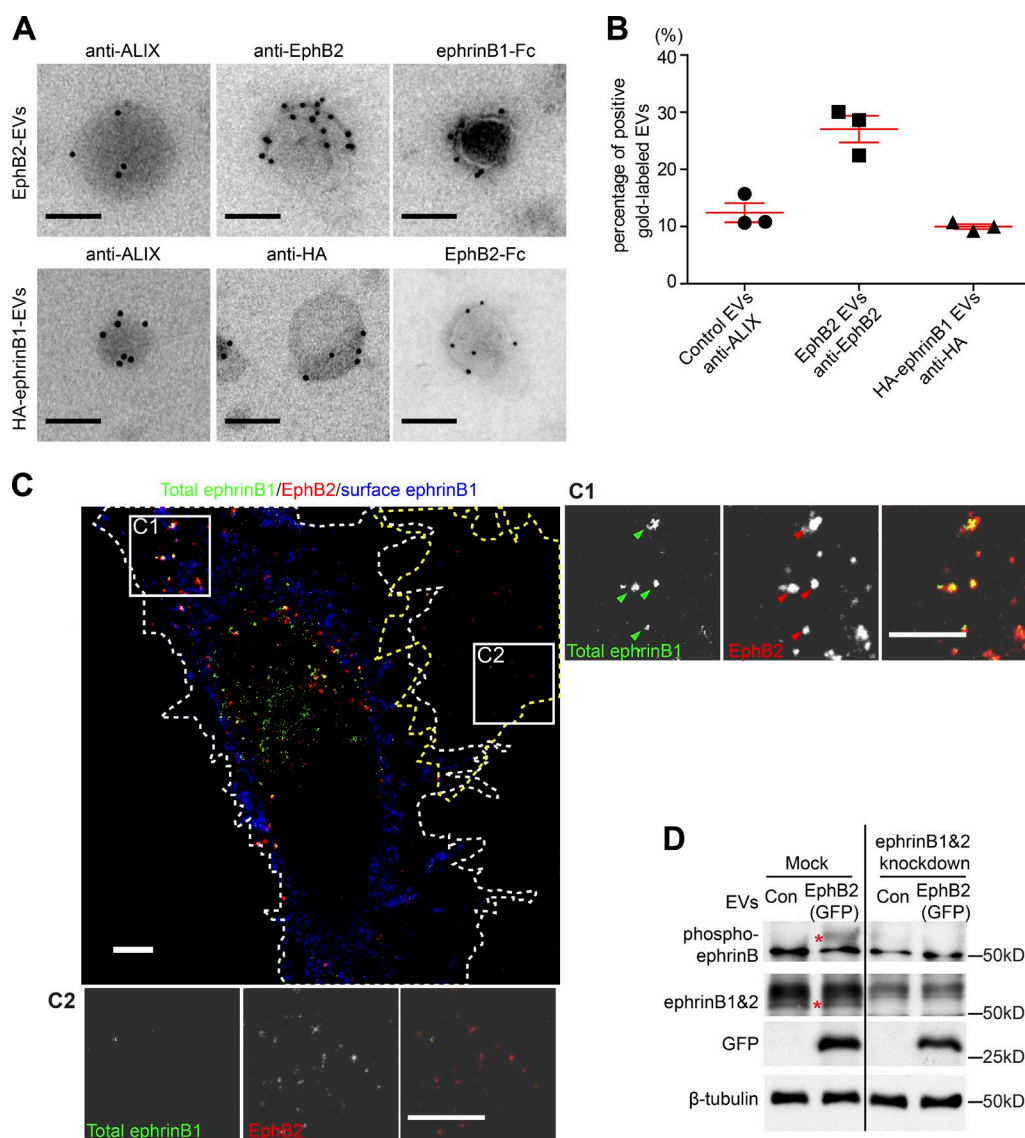
Figure 3. **EphB2⁺ EVs induce ephrinB1 tyrosine phosphorylation.** (A) Representative IEM images of EVs from HEK293 cells stably expressing EphB2 or HA-ephrinB1 with indicated antibodies or Fc proteins. (B) Quantification of the fraction of control, EphB2⁺, and ephrinB1⁺ EVs with gold particles after staining with the indicated antibodies (from three separate EV preparations and IEM experiments). (C) Representative image and higher-power insets showing stronger EphB2⁺ EV signal on an ephrinB1-positive (white dashed outline, C1) compared with ephrinB1-negative cell (yellow dashed outline, C2). EphB2⁺ EVs cluster and colocalize with ephrinB1 (arrowheads in C1). HeLa cells overexpressing HA-ephrinB1-CFP were treated with EphB2⁺ EVs for 2 h and fixed, and surface ephrinB1 was immunolabeled with HA antibody without permeabilization. Cells were then permeabilized and immunolabeled with EphB2 antibody. (D) EphB2⁺ EVs induce endogenous ephrinB1 and ephrinB2 phosphorylation. SKN cells were either mock-transfected or subjected to RNAi-mediated knockdown of ephrinB1 and ephrinB2 (mean knock-down efficiency was 60%; $n = 3$) followed by treatment with control or EphB2⁺ EVs for 2 h. Red asterisks mark the positions of indicated proteins. GFP was used to monitor EphB2⁺ EVs isolated from HEK293 cells stably expressing both EphB2 and membrane-targeted GFP. Similar results were observed in three independent replicates. Bars: (A) 100 nm; (C) 5 µm.

may play a role at active synapses. This could be particularly relevant at the hippocampal CA3-CA1 synapse, where EphB2 (Dalva et al., 2000) and ephrinB2/B3 (Grunwald et al., 2004) are required for long-term potentiation in the postsynaptic dendrite rather than in a trans-synaptic configuration (Klein, 2009). Activity-dependent EV release of EphB2 or ephrinBs may trigger ephrinB-EphB signaling and potentiate synaptic transmission.

Finally, Ephs and their ligands are important modulators of the cancer microenvironment through very diverse mechanisms and are currently being therapeutically targeted for anticancer treatment (Boyd et al., 2014; Barquilla and Pasquale, 2015). That they are present in EVs from different cancer cells (Li et al., 2013; Tauro et al., 2013) raises the possibility that

ephrin-Eph contact-independent signaling contributes to this diversity. Strategies aimed at modulating the secretion of EVs may interfere with ephrin-Eph signaling and thus have tumor-suppressive effects.

Materials and methods

Antibodies and reagents

Antibodies used were as follows: anti–ephrin-B1 (SC-910, rabbit polyclonal; Santa Cruz Biotechnology, Inc.), anti-EphB2 (AF467, goat polyclonal; R&D Systems), anti-EphB1/B2 (phospho-Y594; ab61791, rabbit polyclonal; Abcam), M2 anti-FLAG (F3165, mouse
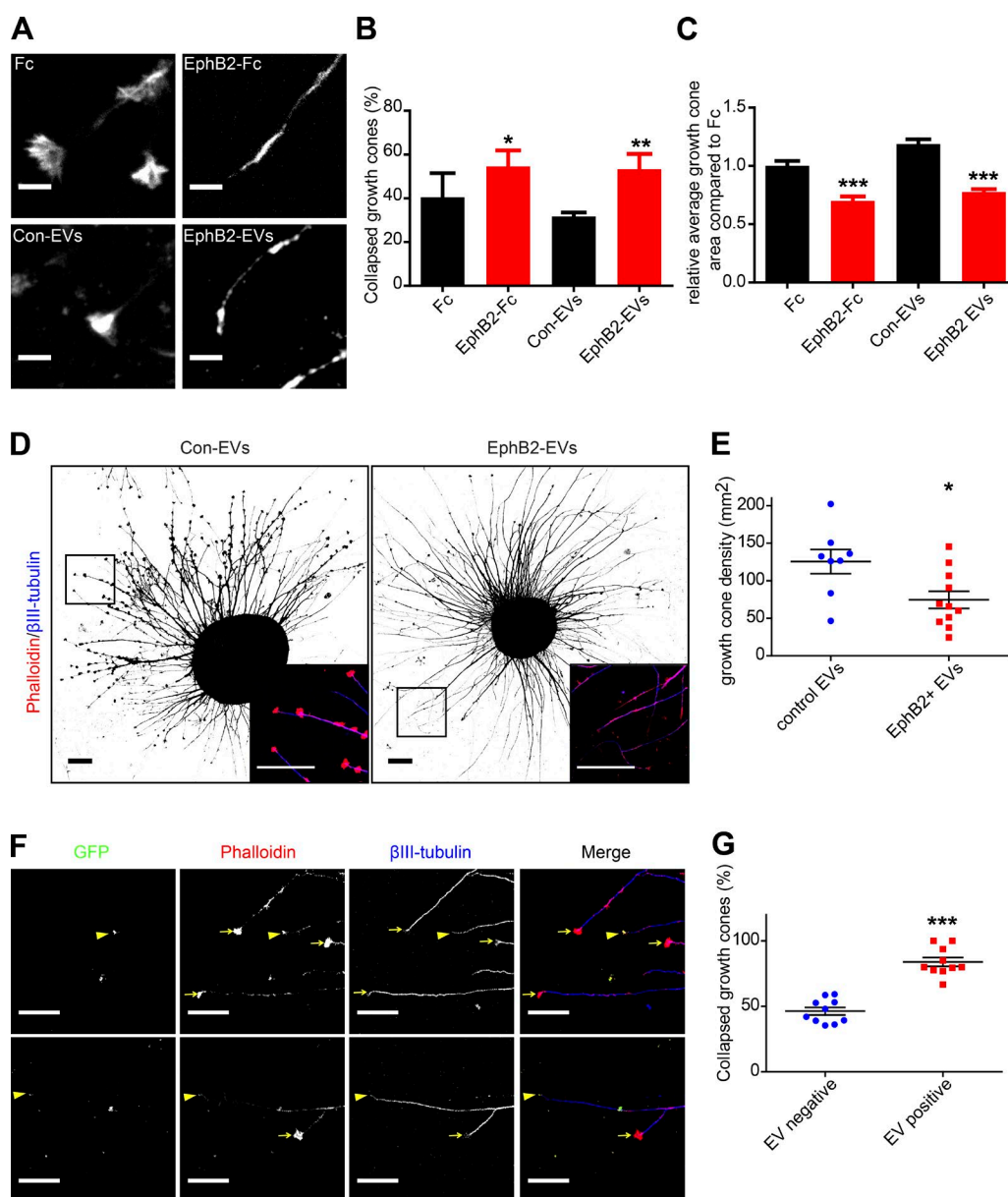
Figure 4. **EphB2+ EVs induce growth cone collapse.** (A) Representative images showing growth cone collapse of dissociated forebrain neurons (3 DIV) triggered either by EphB2-Fc compared with Fc control or by EphB2+ EVs compared with control EVs (Con EVs). (B and C) Quantification of the percentage of collapsed growth cones (B; mean ± SD) and mean growth cone area (C; mean ± SEM; from three individual cultures, of ≥240 growth cones per condition as described in A, one-way analysis of variance). (D) Representative images of E15.5 mouse motor cortex explants (3 DIV) treated with control (Con-EVs) or EphB2+ EVs (EphB2-EVs) for 3 h. Inverted images of phalloidin stainings are shown. High-power insets: the boxed regions with merged βIII-tubulin and phalloidin signal. (E) Quantification of growth cone density of the explants (from three individual explant cultures as described in D and ≥350 growth cones from ≥8 explants per condition were counted, mean ± SEM, two-tailed Student's *t* test). (F) Representative images showing that phalloidin/βIII-tubulin–stained growth cones in contact with GFP+, EphB2+ EVs (arrowheads) collapsed, whereas those free of EV contact (arrows) are spread out. Experimental design as described for D. (G) Quantification of the percentage of collapsed growth cones with or without EV contact (from three individual cultures as described in F and 745 growth cones from 10 explants counted, mean ± SEM, two-tailed Student's *t* test). Bars: (A) 10 µm; (D) 100 µm; (F) 50 µm.

monoclonal; Sigma-Aldrich), anti-FLAG (F7425 rabbit polyclonal; Sigma-Aldrich), anti-ephrinB (ab55352, rabbit polyclonal; Abcam), anti–phospho-ephrinB (3481, rabbit polyclonal; Cell Signaling Technology), 4G10 (05-321, mouse monoclonal; EMD Millipore), anti-ALIX (3A9, mouse monoclonal; Santa Cruz Biotechnology, Inc.), anti-CD63/LAMP3 (MA5-11501, mouse monoclonal; Thermo Fisher Scientific), anti-Flotillin1 (ab41927, rabbit polyclonal; Abcam), anti-Flotillin2 (ab96507, rabbit polyclonal; Abcam), anti-CHMP4B (C-12, rabbit polyclonal; Santa Cruz Biotechnology, Inc.), anti-STAM (29C678, mouse monoclonal; Thermo Fisher

Scientific), anti-HA (ab18181, mouse monoclonal; Abcam), anti-VpsA (SAB4200022, rabbit polyclonal; Sigma-Aldrich), and rabbit serum (R9133; Sigma-Aldrich).

Human IgG Fc fragment was purchased from Jackson Immuno-Research Laboratories, Inc. Mouse ephrinB1-Fc, human EphB2-Fc, and human ephrinA5-Fc fusion proteins (R&D Systems) were used for stimulations and IEM staining. For Fc preclustering, Fc fragment, ephrinB1-Fc, ephrinA5-Fc, or EphB2-Fc fusion proteins were incubated with goat anti–human Fc at a ratio of 5:1 for 30 min at RT (Zimmer et al., 2003).
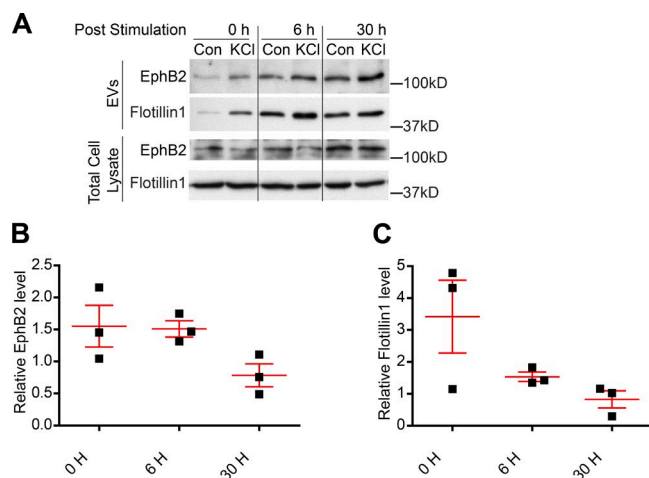
Figure 5. Membrane depolarization enhances EphB2 release via EVs. (A) Western blot (WB) analysis of TCL and purified EVs from E15.5 dissociated cortical neurons (14 DIV) either kept in basal medium (containing 5 mM KCl; con) or substituted with 25 mM KCl for 1 h. Media were collected either immediately after high KCl treatment (0 h) or after the indicated time points and subjected to EV purification. (B and C) EphB2 (B) and Flotillin1 (C) levels increased in EVs after KCl treatment at the 0- and 6-h time points compared with control treatment (from EV preparations of three individual cultures; mean ± SEM).

Plasmid DNA construction

Expression constructs encoding murine full-length and C-terminally truncated EphB2-YFP have been described previously (Zimmer et al., 2003) and served as starting plasmids for Avi-tag insertion downstream of FLAG in the N-terminal of the EphB2 ectodomain. For full-length EphB2-YFP, EYFP was cloned in frame into the juxtamembrane region of FLAG-EphB2 with the flanking amino acid sequence as ...GFERADSE-(EYFP)-YTDKLQHY.... For C-terminally truncated EphB2-YFP (EphB2-YFP-ΔC), the remaining amino acid sequence of the EphB2 cytoplasmic domain is ...GFERADSE and is followed by the EYFP sequence. Full-length cDNA encoding various ESCRT complex proteins (STAM, VPS4A, and CHMP4B) was cloned from cDNA of HeLa cells and subcloned into pEGFP-C1 vectors. Amino acid substitution in VPS4A (dominant-negative VPS4A [E228Q]) was generated by PCR site-directed mutagenesis from wild-type VPS4A. All constructs were sequence verified and tested for correct expression.

Cell culture and transfection

HEK293 (CRL-1573; ATCC) and HeLa (CCL-2; ATCC) cells were cultured in DMEM (Gibco) containing 10% fetal bovine serum (Gibco). Cells were transfected using Lipofectamine 2000 (Thermo Fisher Scientific) or FUGENE6 (Roche) according to the manufacturer's protocol. HEK293 cell lines stably expressing HA-ephrin-B1 or EphB2 and membrane targeted myristoylated GFP (EphB2 [GFP]) have been described previously (Jørgensen et al., 2009). SK-N-BE(2) cells (human neuroblastoma, CRL-2271; ATCC) were cultured in reduced serum medium (Opti-MEM, GlutaMAX Supplement; Gibco) containing 10% FBS (Gibco).

U251 cells (09063001-1VL; Sigma-Aldrich) were cultured in MEM (Gibco) containing 10% FBS (Gibco), 2 mM glutamine, 1% nonessential amino acids, and 1 mM sodium pyruvate. All cell lines tested negative for mycoplasma contamination.

Primary forebrain neurons and cortical neurons were dissected from E15.5 mouse embryos, plated onto cell culture dishes coated with 1 mg/ml poly-ᴅ-lysine (Sigma-Aldrich) and 5 µg/ml laminin (Thermo Fisher Scientific), and cultured in Neurobasal-B27 medium (Gibco; Lauterbach and Klein, 2006).

SILAC labeling

DMEM deficient in arginine and lysine was purchased from PAA Laboratories, as was dialyzed FCS; penicillin/streptomycin was from Gibco. SILAC media were prepared with 10% dialyzed FCS, penicillin/streptomycin, and 50 mg/l arginine and lysine. To prepare light (L), medium (M), and heavy (H) media, the following amino acids were added: for L, Arg0 and Lys0 (arginine and lysine; Sigma-Aldrich); for M, Arg6 and Lys4 (Arg-13C6 and Lys-4,5,5,5-d4; Cambridge Isotope Laboratories); for H, Arg10 and Lys8 (Arg-13C6,15N4 and Lys-13C6,15N2; Cambridge Isotope Laboratories). Cells were grown for a minimum of three passages in this medium. Labeling efficiency was calculated to be higher than 95%. No proline conversion was observed upon inspection of acquired MS data.

Purification of biotinylated EphB2 interaction proteins

Expression levels of FLAG-Avi-tagged full-length EphB2 and EphB2-ΔC were adjusted such that their ratio was nearly 1. To do this, 1.5 µg of plasmid encoding FLAG-Avi–tagged full-length EphB2 or 0.5 µg of plasmid encoding FLAG-Avi-tagged EphB2ΔC was transfected into HeLa cells cultured in 100-mm dishes using Lipofectamine 2000 (Thermo Fisher Scientific). Site-specific EphB2 biotinylation was achieved by adding BirA to the culture media (Howarth and Ting, 2008). Cells expressing FLAG-Avi–tagged full-length EphB2 without BirA addition were used as unbiotinylated control. 30 µl of streptavidin-conjugated Dynabeads (Dynabeads M-280 Streptavidin; Thermo Fisher Scientific) were added per dish to induce EphB2 clustering. Cells were washed twice with DMEM after incubation with Dynabeads for 30 min at 37°C. Cells were then treated with 0.5 mM dithiobis(succinimidyl propionate) (DSP) at RT for 5 min. DSP was quenched by incubating cells with ice-cold PBS containing 50 mM Tris-HCl (three times, 5 min each time). Cells were then collected in Lysis buffer (50 mM Tris-HCl, pH 8.0, 150 mM NaCl, 5 mM EDTA, 1.25% Triton X-100, 0.25% SDS, and 5 mg/ml iodoacetamide), and EphB2 interaction protein complex was purified by Dynabeads and used for liquid chromatography/mass spectrometry.

Protein digestion and peptide fractionation

Protein samples were digested by trypsin (proteomics grade; Roche) using the filter-assisted sample preparation method and separated on anion exchange microcolumns, essentially as reported (Wiśniewski et al., 2009, 2011). Finally, peptides were desalted, filtered, and enriched as previously described (Rappsilber et al., 2003) and dried in a vacuum centrifuge.

Peptide separation and mass spectrometry for SILAC-immunoprecipitation experiments

Purified peptide fractions were dissolved in 5% (vol/vol) formic acid and sonicated for 5 min. Samples were analyzed on a nanoACQUITY HPLC system (Waters) coupled to a LTQ-Orbitrap mass spectrometer (Thermo Fisher Scientific). Peptides were separated on homemade spray-columns (internal diameter 75 µm, length 20 cm, tip opening 8 µm; NewObjective) packed with 3-µm C18 particles (Reprosil-Pur C18-AQ; Dr. Maisch) using a 2-h stepwise gradient between 5% buffer A (0.2% formic acid in water) and 60% buffer B (0.2% formic acid in acetonitrile). Samples were loaded on the column by the nanoACQUITY autosampler at a flow rate of 0.5 µl/min. No trap column was used. The HPLC flow rate was set to 0.2 µl/min during analysis. MS/MS analysis was performed with standard settings using cycles of one high-resolution (60,000 full width at half-maximum [FWHM]) MS scan followed by eight MS/MS scans of the eight most intense ions with charge states of 2 or higher.

Peptide separation and mass spectrometry for exosome/EV analyses

Peptides eluted from desalting tips were dissolved in 5% (vol/vol) formic acid and sonicated for 5 min. Samples were analyzed on an EASY-nLC 1000 HPLC system (Thermo Fisher Scientific) coupled to a Q-Exactive mass spectrometer (Thermo Fisher Scientific). Peptides were separated on homemade spray-columns (internal diameter, 75 µm; length, 20 cm; tip opening, 8 µm; New Objective) packed with 1.9-µm C18 particles (Reprosil-Pur C18-AQ) using a 2-h stepwise gradient between 5% buffer A (0.2% formic acid in water) and 60% buffer B (0.1% formic acid in acetonitrile). Samples were loaded on the column by the nanoACQUITY autosampler at a flow rate of 0.5 µl/min. No trap column was used. The HPLC flow rate was set to 0.25 µl/min during analysis. MS/MS analysis was performed with standard settings using cycles of one high-resolution (70,000 FWHM setting) MS scan followed by 10 MS/MS scans of the 10 most intense ions with charge states of 2 or higher at a resolution setting of 17,500 FWHM.

Analysis of MS data

Protein identification and SILAC-based quantitation were performed using MaxQuant (version 1.3.0.5) with default settings. Human sequences of UNIPROT (version 2011-02-14) were used as a database for SILAC immunoprecipitation analyses, whereas the UNIPROT reference proteome databases for human and mouse (versions 2014-04) were searched for protein identification from purified exosomes from U-251 MG cells and cultured cortical neurons, respectively. MaxQuant used a decoy version of the specified UNIPROT databases to adjust the false discovery rates for proteins and peptides of less than 1%.

Coimmunoprecipitation

HEK293 cells stably expressing EphB2 and membrane targeted myristoylated GFP were used to detect the interaction between EphB2 and endogenous STAM or VPS4A. Cells were washed twice with PBS and lysed in immunoprecipitation buffer (25 mM Hepes, pH 7.4, 150 mM NaCl, 1 mM EDTA, 1 mM EGTA, and 1% *n*-dodecyl-β-D-maltoside) by sonication. Cell lysates were cleared by centrifugation and then incubated with protein G Sepharose 4 fast flow beads (GE Healthcare) supplemented with anti-EphB2 antibodies (positive control), rabbit serum (negative control), and anti-STAM antibodies or anti-VPS4A antibodies for at least 3 h at 4°C, washed three times with lysis buffer, and analyzed by Western blot.

For coimmunoprecipitation (co-IP) experiments in HeLa cells, 1 µg plasmid expressing STAM-GFP, CHMP4B-GFP, or VPS4A-GFP was cotransfected with 1 µg plasmid expressing full-length FLAG-EphB2-YFP or FLAG-YFP (as negative control) using Lipofectamine 2000 (Thermo Fisher Scientific). 24 h after transfection, cells were washed twice with PBS and lysed in immunoprecipitation buffer (25 mM Hepes, pH 7.4, 150 mM NaCl, 1 mM EDTA, 1 mM EGTA, and 1% Triton X-100) by sonication. Cell lysates were cleared by centrifugation and incubated with anti-FLAG M2-Agarose resin (Sigma-Aldrich) for at least 3 h at 4°C, washed four times with lysis buffer, and analyzed by Western blot with the indicated specific antibodies. All co-IP experiments were replicated at least three times with similar results.

Immunocytochemistry

Cells were fixed with prewarmed 4% paraformaldehyde and 8% sucrose in D-PBS for 20 min at RT, rinsed twice with ice-cold D-PBS, incubated with 50 mM ice-cold ammonium chloride in D-PBS for 10 min, and rinsed again. For surface labeling of Ephs or ephrins, cells were not permeabilized. Blocking was performed for 30 min at RT with blocking solution (4% goat serum, 4% donkey serum, and 2% BSA in PBS), followed by incubation with the primary antibodies in blocking solution for 2 h at RT. For further total labeling, cells were permeabilized with 0.1% Triton X-100 for 5 min and incubated with blocking solution for 1 h at RT, followed by incubation with the primary antibodies in blocking solution for 2 h at RT. After washing with PBS, secondary antibodies diluted 1:250 in blocking solution were applied for 1 h at RT. After washing, coverslips were mounted using the ProLong antifade kit (Thermo Fisher Scientific).

Exosome/EV purification

Exosomes/EVs were isolated from the conditioned medium (supplied with 10% exosome-depleted FBS [BIO-CAT]) of U251 cells, parental HEK293 cells, HEK293 cells stably expressing EphB2 and membrane targeted GFP, or HA-ephrinB1. Culture medium from cultured primary cortical neurons (14 DIV) was used for exosome/EV purification. In the case of neuron activation, cultured primary cortical neurons (14 DIV) were washed with NeuroBasal medium and stimulated with 25 mM KCl in Neurobasal-B27 medium for 1 h. Cells were washed three times with NeuroBasal medium, and fresh Neurobasal-B27 medium was added. Stimulation medium, medium from 6 and 30 h after stimulation, was used for exosome/EV purification.

Exosomes/EVs were purified as previously described using serial centrifugation (Thery et al., 2006). In brief, conditioned medium was sequentially centrifuged for 10 min at 300 *g*, 10 min at 2,000 *g*, and 30 min at 10,000 *g*. The resulting supernatant was filtered through a 0.22-µm filter and centrifuged for 150 min at 100,000 *g*. The pellet was resuspended in PBS containing 25 mM Hepes, pH 7.2, and centrifuged again for 100 min at 100,000 *g*. The P100 exosome/EV-containing pellet was resuspended in PBS containing 25 mM Hepes, pH 7.2. Protein concentrations of the P100 fraction were determined with a MicroBCA protein reagent kit (Thermo Fisher Scientific) using BSA as the standard. Purified P100 fractions were further analyzed using Western blotting, EM, or cell treatments.

EM

EM analysis of exosomes/EVs was performed as previously described (Thery et al., 2006). For whole mounted exosomes/EVs, the P100 fraction was fixed with 4% PFA, applied to formvar carbon–coated EM grids, and negatively stained with uranyl-oxalate, pH 7. The negative-stained grids were then incubated in methylcellulose–uranyl acetate solution on ice. The solution was removed by wicking onto filter paper. Immunogold labeling of exosomes/EVs was performed using anti-CD63, anti-HA, anti-EphB2, EphB2-Fc, or ephrinB1-Fc, followed by labeling with a gold-conjugated secondary antibody (25705; EMS). Air-dried grids were visualized with a transmission electron microscope operating at 80 KeV. For ALIX staining, exosomes/EVs were permeabilized and stained as previously described (Korkut et al., 2013).

Image acquisition and procession

Images were acquired at RT either on a confocal laser scanning microscope (LSM780; ZEISS) equipped with a Plan-APO 63×/NA1.46 oil-immersion objective (ZEISS) using Zen software or on a Zeiss Axio Observer Z1 inverted microscope (ZEISS) equipped with a CSU-X1 spinning disc confocal unit (Yokogawa Electric Corporation) controlled by VisiView software (Visitron Systems) and a CoolSnapHQ2 CCD camera (Photometrics) using a Plan-APO 40×/NA1.4 oil-immersion objective. Excitation was provided by lasers of 405-, 488-, 561-, or 640-nm wavelength (Visitron Systems). For visualization purposes, all images are presented after intensity adjustment using Fiji or Photoshop (Adobe Systems). All adjustments within an experiment were performed equally.

Quantification of STAM and CHMP4B signal at the plasma membrane

HeLa cells overexpressing FLAG-tagged full-length EphB2-YFP were fixed, and surface EphB2 was immunolabeled with anti-FLAG

antibodies before permeabilization. The total pool of STAM or CHMP4B was immunolabeled after permeabilization. To quantify the plasma membrane fraction of STAM and CHMP4B, images were Gaussian-blurred and thresholded to generate a binary mask. The binary masks were manually adjusted to align with the cell edges. Fluorescence intensity within a 4-pixel-thick area along the edge of the mask was defined as the plasma membrane fraction, and the rest of the intensities were defined as the intracellular fraction. Data were collected from three independent replicates with at least three pairs of cells (EphB2-positive cell versus EphB2-negative cell) to calculate the fold increase of STAM or CHMP4B levels at the plasma membrane.

Quantification of ephrinB1 and ephrinB2 knockdown efficiency
SKN cells, which endogenously express both ephrinB1 and ephrinB2, were either mock-transfected or subjected to RNAi-mediated knockdown of ephrinB1 and ephrinB2. 24 h later, cells were further incubated with control or EphB2$^+$ EVs for 2 h. Total cell lysates were subjected to Western blot analysis. The intensity of ephrinB levels was indicated by anti-ephrinB1 and -2 antibodies, which recognize both ephrinB1 and ephrinB2. Knockdown efficiency was calculated by comparing the level of ephrinB1 and ephrinB2 after ephrinB1 and ephrinB2 siRNA treatment with mock treatment (both under control exosome treatment conditions). Mean knockdown efficiency was calculated from three independent experiments.

Growth cone collapse analysis
Dissociated forebrain neurons, cortical neurons, and motor cortex explant cultures (E15.5) were generated as previously described (Seiradake et al., 2014). In Fig. 4 (A–C), primary E15.5 forebrain neurons dissociated and cultured for 3 d were treated with 1 µg/ml preclustered human-Fc or EphB2-Fc for 30 min or treated with control EVs (Con-EVs) or EphB2$^+$ EVs (EphB2-EVs) for 3 h. Cells were fixed and stained with phalloidin. EphB2$^+$ EVs were isolated from HEK293 cells stably expressing both EphB2 and membrane-targeted GFP. In Fig. 4 (D–G), motor cortex explants cultured for 3 d were incubated with exosomes/EVs purified from HEK293 cells with (EphB2-EV) or without (control-EV) stable EphB2 and membrane-targeted GFP expression. After 3-h incubation at 37°C, explants were fixed with 4% PFA for 20 min at RT and labeled with βIII-tubulin (1/1,000; Sigma-Aldrich) and Alexa Fluor 568–phalloidin (1/500; Thermo Fisher Scientific) after permeabilization to analyze growth cone morphologies. Quantification of growth cone collapse was done as previously described (Seiradake et al., 2014).

Statistical analysis
Statistical analysis was performed in GraphPad Prism software (version 5.00). Results were reported either by mean ± SEM or mean ± SD as indicated in the figure legends. No statistical method was used to predetermine sample size. The datasets with data points higher than 5 were analyzed with the D'Agostino and Pearson omnibus normality test. Datasets with normal distributions were analyzed with either Student's t test to compare two conditions or one-way analysis of variance Tukey test to compare multiple conditions. Datasets that did not follow a normal distribution in the normality test were analyzed with Kruskal–Wallis test (multiple comparison). For data with replicates less than five, we assumed normal distribution based on the appearance of the data and analyzed with Student's t test.

Online supplemental material
Table S1 provides the full list of proteins identified in all three SILAC experiments. Table S2 provides the original mass spectrometry dataset for the full list of proteins identified in EVs purified from U-251MG glioblastoma cells. Table S3 provides the original mass spectrometry dataset for the full list of proteins identified in EVs purified from E15.5 dissociated motor cortex neurons (14 DIV). Table S4 provides detailed information of all identified peptides corresponding to Eph or ephrin from EVs purified from E15.5 dissociated motor cortex neurons (14 DIV). Fig. S1 is related to Fig. 1, showing that ESCRT complex components are EphB2 interactors. Fig. S2 is related to Figs. 2 and 3, showing the characteristics of EVs purified from HEK293 cells stably expressing EphB2 or ephrinB1. Online supplemental material is available at http://www.jcb.org/cgi/content/full/jcb.201601085/DC1.

References

Bahrini, I., J.H. Song, D. Diez, and R. Hanayama. 2015. Neuronal exosomes facilitate synaptic pruning by up-regulating complement factors in microglia. *Sci. Rep.* 5:7989. http://dx.doi.org/10.1038/srep07989

Barile, L., V. Lionetti, E. Cervio, M. Matteucci, M. Gherghiceanu, L.M. Popescu, T. Torre, F. Siclari, T. Moccetti, and G. Vassalli. 2014. Extracellular vesicles from human cardiac progenitor cells inhibit cardiomyocyte apoptosis and improve cardiac function after myocardial infarction. *Cardiovasc. Res.* 103:530–541. http://dx.doi.org/10.1093/cvr/cvu167

Barquilla, A., and E.B. Pasquale. 2015. Eph receptors and ephrins: Therapeutic opportunities. *Annu. Rev. Pharmacol. Toxicol.* 55:465–487. http://dx.doi.org/10.1146/annurev-pharmtox-011112-140226

Boyd, A.W., P.F. Bartlett, and M. Lackmann. 2014. Therapeutic targeting of EPH receptors and their ligands. *Nat. Rev. Drug Discov.* 13:39–62. http://dx.doi.org/10.1038/nrd4175

Colombo, M., C. Moita, G. van Niel, J. Kowal, J. Vigneron, P. Benaroch, N. Manel, L.F. Moita, C. Théry, and G. Raposo. 2013. Analysis of ESCRT functions in exosome biogenesis, composition and secretion highlights the heterogeneity of extracellular vesicles. *J. Cell Sci.* 126:5553–5565. http://dx.doi.org/10.1242/jcs.128868

Colombo, M., G. Raposo, and C. Théry. 2014. Biogenesis, secretion, and intercellular interactions of exosomes and other extracellular vesicles. *Annu. Rev. Cell Dev. Biol.* 30:255–289. http://dx.doi.org/10.1146/annurev-cellbio-101512-122326

Dalva, M.B., M.A. Takasu, M.Z. Lin, S.M. Shamah, L. Hu, N.W. Gale, and M.E. Greenberg. 2000. EphB receptors interact with NMDA receptors and regulate excitatory synapse formation. *Cell.* 103:945–956. http://dx.doi.org/10.1016/S0092-8674(00)00197-5

Davis, S., N.W. Gale, T.H. Aldrich, P.C. Maisonpierre, V. Lhotak, T. Pawson, M. Goldfarb, and G.D. Yancopoulos. 1994. Ligands for EPH-related receptor tyrosine kinases that require membrane attachment or clustering for activity. *Science.* 266:816–819. http://dx.doi.org/10.1126/science.7973638

Fauré, J., G. Lachenal, M. Court, J. Hirrlinger, C. Chatellard-Causse, B. Blot, J. Grange, G. Schoehn, Y. Goldberg, V. Boyer, et al. 2006. Exosomes are released by cultured cortical neurones. *Mol. Cell. Neurosci.* 31:642–648. http://dx.doi.org/10.1016/j.mcn.2005.12.003

Gatto, G., D. Morales, A. Kania, and R. Klein. 2014. EphA4 receptor shedding regulates spinal motor axon guidance. *Curr. Biol.* 24:2355–2365. http://dx.doi.org/10.1016/j.cub.2014.08.028

Georgakopoulos, A., C. Litterst, E. Ghersi, L. Baki, C. Xu, G. Serban, and N.K. Robakis. 2006. Metalloproteinase/Presenilin1 processing of ephrinB regulates EphB-induced Src phosphorylation and signaling. *EMBO J.* 25:1242–1252. http://dx.doi.org/10.1038/sj.emboj.7601031

Gradilla, A.C., E. González, I. Seijo, G. Andrés, M. Bischoff, L. González-Mendez, V. Sánchez, A. Callejo, C. Ibáñez, M. Guerra, et al. 2014. Exosomes as Hedgehog carriers in cytoneme-mediated transport and secretion. *Nat. Commun.* 5:5649. http://dx.doi.org/10.1038/ncomms6649

Gross, J.C., V. Chaudhary, K. Bartscherer, and M. Boutros. 2012. Active Wnt proteins are secreted on exosomes. *Nat. Cell Biol.* 14:1036–1045. http://dx.doi.org/10.1038/ncb2574

Grunwald, I.C., M. Korte, G. Adelmann, A. Plueck, K. Kullander, R.H. Adams, M. Frotscher, T. Bonhoeffer, and R. Klein. 2004. Hippocampal plasticity requires postsynaptic ephrinBs. *Nat. Neurosci.* 7:33–40. http://dx.doi.org/10.1038/nn1164

Hattori, M., M. Osterfield, and J.G. Flanagan. 2000. Regulated cleavage of a contact-mediated axon repellent. *Science.* 289:1360–1365. http://dx.doi.org/10.1126/science.289.5483.1360

Howarth, M., and A.Y. Ting. 2008. Imaging proteins in live mammalian cells with biotin ligase and monovalent streptavidin. *Nat. Protoc.* 3:534–545. http://dx.doi.org/10.1038/nprot.2008.20

Janes, P.W., N. Saha, W.A. Barton, M.V. Kolev, S.H. Wimmer-Kleikamp, E. Nievergall, C.P. Blobel, J.P. Himanen, M. Lackmann, and D.B. Nikolov. 2005. Adam meets Eph: an ADAM substrate recognition module acts as a molecular switch for ephrin cleavage in trans. *Cell.* 123:291–304. http://dx.doi.org/10.1016/j.cell.2005.08.014

Janes, P.W., S.H. Wimmer-Kleikamp, A.S. Frangakis, K. Treble, B. Griesshaber, O. Sabet, M. Grabenbauer, A.Y. Ting, P. Saftig, P.I. Bastiaens, and M. Lackmann. 2009. Cytoplasmic relaxation of active Eph controls ephrin shedding by ADAM10. *PLoS Biol.* 7:e1000215. http://dx.doi.org/10.1371/journal.pbio.1000215

Jørgensen, C., A. Sherman, G.I. Chen, A. Pasculescu, A. Poliakov, M. Hsiung, B. Larsen, D.G. Wilkinson, R. Linding, and T. Pawson. 2009. Cell-specific information processing in segregating populations of Eph receptor ephrin-expressing cells. *Science.* 326:1502–1509. http://dx.doi.org/10.1126/science.1176615

Klein, R. 2009. Bidirectional modulation of synaptic functions by Eph/ephrin signaling. *Nat. Neurosci.* 12:15–20. http://dx.doi.org/10.1038/nn.2231

Klein, R., and A. Kania. 2014. Ephrin signalling in the developing nervous system. *Curr. Opin. Neurobiol.* 27:16–24. http://dx.doi.org/10.1016/j.conb.2014.02.006

Korkut, C., Y. Li, K. Koles, C. Brewer, J. Ashley, M. Yoshihara, and V. Budnik. 2013. Regulation of postsynaptic retrograde signaling by presynaptic exosome release. *Neuron.* 77:1039–1046. http://dx.doi.org/10.1016/j.neuron.2013.01.013

Kunadt, M., K. Eckermann, A. Stuendl, J. Gong, B. Russo, K. Strauss, S. Rai, S. Kügler, L. Falomir Lockhart, M. Schwalbe, et al. 2015. Extracellular vesicle sorting of α-Synuclein is regulated by sumoylation. *Acta Neuropathol.* 129:695–713. http://dx.doi.org/10.1007/s00401-015-1408-1

Lauterbach, J., and R. Klein. 2006. Release of full-length EphB2 receptors from hippocampal neurons to cocultured glial cells. *J. Neurosci.* 26:11575–11581. http://dx.doi.org/10.1523/JNEUROSCI.2697-06.2006

Li, W., D. Mu, F. Tian, Y. Hu, T. Jiang, Y. Han, J. Chen, G. Han, and X. Li. 2013. Exosomes derived from Rab27a-overexpressing tumor cells elicit efficient induction of antitumor immunity. *Mol. Med. Rep.* 8:1876–1882. http://dx.doi.org/10.3892/mmr.2013.1738

Marston, D.J., S. Dickinson, and C.D. Nobes. 2003. Rac-dependent trans-endocytosis of ephrinBs regulates Eph-ephrin contact repulsion. *Nat. Cell Biol.* 5:879–888. http://dx.doi.org/10.1038/ncb1044

Nievergall, E., P.W. Janes, C. Stegmayer, M.E. Vail, F.G. Haj, S.W. Teng, B.G. Neel, P.I. Bastiaens, and M. Lackmann. 2010. PTP1B regulates Eph receptor function and trafficking. *J. Cell Biol.* 191:1189–1203. http://dx.doi.org/10.1083/jcb.201005035

Ong, S.E., B. Blagoev, I. Kratchmarova, D.B. Kristensen, H. Steen, A. Pandey, and M. Mann. 2002. Stable isotope labeling by amino acids in cell culture, SILAC, as a simple and accurate approach to expression proteomics. *Mol. Cell. Proteomics.* 1:376–386. http://dx.doi.org/10.1074/mcp.M200025-MCP200

Rajendran, L., J. Bali, M.M. Barr, F.A. Court, E.M. Krämer-Albers, F. Picou, G. Raposo, K.E. van der Vos, G. van Niel, J. Wang, and X.O. Breakefield. 2014. Emerging roles of extracellular vesicles in the nervous system. *J. Neurosci.* 34:15482–15489. http://dx.doi.org/10.1523/JNEUROSCI.3258-14.2014

Rappsilber, J., Y. Ishihama, and M. Mann. 2003. Stop and go extraction tips for matrix-assisted laser desorption/ionization, nanoelectrospray, and LC/MS sample pretreatment in proteomics. *Anal. Chem.* 75:663–670. http://dx.doi.org/10.1021/ac026117i

Rusten, T.E., T. Vaccari, and H. Stenmark. 2011. Shaping development with ESCRTs. *Nat. Cell Biol.* 14:38–45. http://dx.doi.org/10.1038/ncb2381

Schaupp, A., O. Sabet, I. Dudanova, M. Ponserre, P. Bastiaens, and R. Klein. 2014. The composition of EphB2 clusters determines the strength in the cellular repulsion response. *J. Cell Biol.* 204:409–422. http://dx.doi.org/10.1083/jcb.201305037

Seiradake, E., A. Schaupp, D. del Toro Ruiz, R. Kaufmann, N. Mitakidis, K. Harlos, A.R. Aricescu, R. Klein, and E.Y. Jones. 2013. Structurally encoded intraclass differences in EphA clusters drive distinct cell responses. *Nat. Struct. Mol. Biol.* 20:958–964. http://dx.doi.org/10.1038/nsmb.2617

Seiradake, E., D. del Toro, D. Nagel, F. Cop, R. Härtl, T. Ruff, G. Seyit-Bremer, K. Harlos, E.C. Border, A. Acker-Palmer, et al. 2014. FLRT structure: balancing repulsion and cell adhesion in cortical and vascular development. *Neuron.* 84:370–385. http://dx.doi.org/10.1016/j.neuron.2014.10.008

Sheldon, H., E. Heikamp, H. Turley, R. Dragovic, P. Thomas, C.E. Oon, R. Leek, M. Edelmann, B. Kessler, R.C. Sainson, et al. 2010. New mechanism for Notch signaling to endothelium at a distance by Delta-like 4 incorporation into exosomes. *Blood.* 116:2385–2394. http://dx.doi.org/10.1182/blood-2009-08-239228

Simpson, R.J., H. Kalra, and S. Mathivanan. 2012. ExoCarta as a resource for exosomal research. *J. Extracell. Vesicles.* 1:1. http://dx.doi.org/10.3402/jev.v1i0.18374

Tauro, B.J., D.W. Greening, R.A. Mathias, S. Mathivanan, H. Ji, and R.J. Simpson. 2013. Two distinct populations of exosomes are released from LIM1863 colon carcinoma cell-derived organoids. *Mol. Cell. Proteomics.* 12:587–598. http://dx.doi.org/10.1074/mcp.M112.021303

Thery, C., S. Amigorena, G. Raposo, and A. Clayton. 2006. Isolation and characterization of exosomes from cell culture supernatants and biological fluids. *Curr Protoc Cell Biol.* Chapter 3:Unit 3.22.

Tkach, M., and C. Théry. 2016. Communication by extracellular vesicles: Where we are and where we need to go. *Cell.* 164:1226–1232. http://dx.doi.org/10.1016/j.cell.2016.01.043

Wiśniewski, J.R., A. Zougman, and M. Mann. 2009. Combination of FASP and StageTip-based fractionation allows in-depth analysis of the hippocampal membrane proteome. *J. Proteome Res.* 8:5674–5678. http://dx.doi.org/10.1021/pr900748n

Wiśniewski, J.R., D.F. Zielinska, and M. Mann. 2011. Comparison of ultrafiltration units for proteomic and N-glycoproteomic analysis by the filter-aided sample preparation method. *Anal. Biochem.* 410:307–309. http://dx.doi.org/10.1016/j.ab.2010.12.004

Zhuang, G., S. Hunter, Y. Hwang, and J. Chen. 2007. Regulation of EphA2 receptor endocytosis by SHIP2 lipid phosphatase via phosphatidylinositol 3-Kinase-dependent Rac1 activation. *J. Biol. Chem.* 282:2683–2694. http://dx.doi.org/10.1074/jbc.M608509200

Zimmer, M., A. Palmer, J. Köhler, and R. Klein. 2003. EphB-ephrinB bi-directional endocytosis terminates adhesion allowing contact mediated repulsion. *Nat. Cell Biol.* 5:869–878. http://dx.doi.org/10.1038/ncb1045